Chin. Sci. Bull. (2014) 59(18):2073–2091
DOI 10.1007/s11434-014-0237-2

csb.scichina.com
www.springer.com/scp

Review

Materials Science

Recent progress in thermoelectric materials

Chao Han · Zhen Li · Shixue Dou

Received: 13 August 2013 / Accepted: 13 September 2013 / Published online: 15 March 2014

Abstract Direct conversion of heat into electricity through advanced thermoelectric (TE) materials has been one of the most attractive solutions to the severe environmental and energy issues facing humanity. In recent years, great progress has been made in improving their dimensionless figure of merit (*ZT*), which determines the conversion efficiency of TE devices. *ZT* is related to three "interlocked" factors—the Seebeck coefficient, electrical conductivity, and thermal conductivity. These three factors are interdependent in bulk TE materials, and altering one changes the other two. The difficulty in simultaneously optimizing them caused TE research to stagnate, until great reductions in thermal conductivity were both theoretically and experimentally proven in nanomaterials in 1993. In this review, we first introduce some TE fundamentals and then review the most recently improvements in *ZT* in different kinds of inorganic and organic TE materials, which is followed by an investigation of the outlook for new directions in TE technology.

Keywords Thermoelectrics · Functional materials · Nanostructures · Energy conversion

1 Introduction

Growing energy demands, concerns over climate change and depletion of fossil fuel resources have led to a concerted effort to develop sustainable technologies for the efficient use, conversion, and recovery of energy. One such technology is the use of thermoelectric (TE) materials to directly convert heat into electricity, based on the Seebeck effect [1–7], which was discovered in 1836 by Thomas Johann Seebeck. It should be noted that TE materials can also convert electricity into cooling through the Peltier effect. The detailed principles of TE conversions have been described elsewhere [4–7]. This technology has distinct advantages, including: (1) TE conversion is reliable and operates in silence compared with other energy conversion technologies, as it works without mechanical movement; (2) TE devices are simple, compact, and safe; (3) it is an environmentally friendly green technology, because no heat and no gaseous or chemical waste are produced during operation; and (4) it can be widely used in places where other energy conversion technologies are unavailable, such as in the remote outer space [1, 2].

Although TE technology possesses many merits and has been known for more than one century, it has only been applied in narrow fields because of its low conversion efficiency (typically less than 6 %) [6]. The conversion efficiency strongly depends on the figure of merit (*ZT*) of the TE material, as described by Eq. (1),

$$\eta = \eta_c \frac{\sqrt{1+ZT}-1}{\sqrt{1+ZT}+T_c/T_h}, \quad (1)$$

where η is the conversion efficiency of heat to electricity, T_c and T_h are the temperatures of cold and hot sides of a TE generator, respectively, η_c represents the Carnot efficiency and can be expressed as $\eta_c = 1 - T_c/T_h$. *ZT* is given by Eq. (2),

$$ZT = \frac{S^2\sigma T}{\kappa}, \quad (2)$$

where S is the Seebeck coefficient, σ is the electrical conductivity, κ is the thermal conductivity, and $s^2\sigma$ is

SPECIAL ISSUE: Advanced Materials for Clean Energy

C. Han · Z. Li (✉) · S. Dou (✉)
Institute for Superconducting and Electronic Materials, Squires Way, University of Wollongong, Wollongong 2500, NSW, Australia
e-mail: zhenl@uow.edu.au

S. Dou
e-mail: shi_dou@uow.edu.au

called the power factor. The dependence of the conversion efficiency on ZT is shown in Fig. 1. It clearly shows that ZT of TE materials should be at least above 3 in order to ensure that the device conversion efficiency is competitive with that of traditional power generators, which can reach 40 % of Carnot efficiency.

Equation (2) demonstrates that high ZT can be obtained by improving the Seebeck coefficient and electrical conductivity while reducing the thermal conductivity as much as possible. σ of TE materials can be expressed by Eq. (3),

$$\sigma = ne\mu, \tag{3}$$

where n is the density of charge carriers, μ is the mobility of charge carriers, e is the charge of unit carrier. The electrical conductivity can be significantly improved through chemical doping. Each dopant atom can have one more (less) valence electron than its host atoms and hence, can increase the density of charge carriers. Meanwhile, the dopants can also reduce the mobility of the charge carriers due to the enhanced scattering between dopants and carriers. The ideal density of charge carriers should be in a range from 10^{19} to 10^{21} cm^{-3} [8].

Simple doping of impurities may also improve the Seebeck coefficient by changing the electron density of states (DOS) [9]. As shown in Eq. (4),

$$S = \frac{8\pi^2 k_B^2}{3eh^2} m^* T \left(\frac{\pi}{3n}\right)^{2/3}, \tag{4}$$

the Seebeck coefficient is mainly controlled by the carrier concentration and effective mass of the charge carriers (m^*), which usually decreases with increasing carrier mobility. k_B and h are Boltzmann constant and Planck constant, respectively. Another way to enhance the Seebeck coefficient is by the use of external field effects [10].

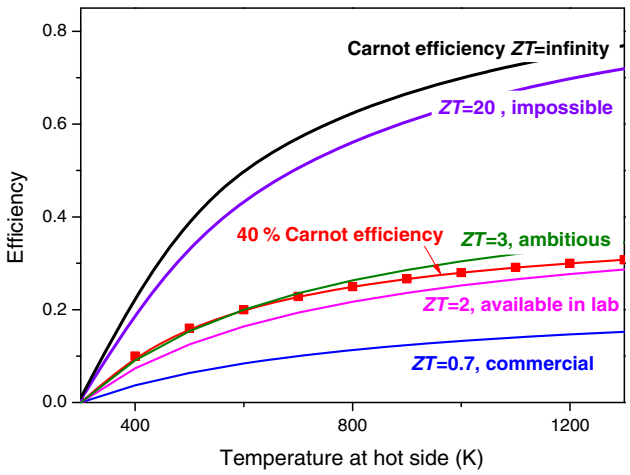

Fig. 1 (Color online) Conversion efficiency of TE materials with changing temperature difference and ZT, assuming that the cold side temperature is 300 K. The red curve is the 40 % Carnot efficiency

Thermal conductivity is decreased by enhancing phonon scattering (i.e., phonon-boundary scattering, phonon-defect scattering, and phonon–phonon scattering). The thermal conductivity includes electron thermal conductivity (k_e) and lattice thermal conductivity (k_c), as shown in Eq. (5),

$$k = k_e + k_c, \tag{5}$$

k_e is proportional to the electrical conductivity according to the Wiedemann–Franz Law [11, 12]. In semiconductors, usually >90 % of thermal conductivity comes from the lattice thermal conductivity (k_c), which is independent of the electrical conductivity. Hence, reducing the lattice thermal conductivity will lead to a pronounced enhancement in the TE performance.

According to the above description, the Seebeck coefficient, the thermal conductivity, and the electrical conductivity are strongly dependent on each other, and it is very challenging to improve them simultaneously in bulk TE materials. Research on TE materials was nearly frozen from the 1960s to the 1990s. In 1993, Dresselhaus and co-workers [13, 14] theoretically proved that low-dimensional materials can have higher ZT than their bulk analogs due both to their lower thermal conductivity and to quantum confinement effects. Their work rekindled research interest in TE materials and provided a strategy to improve the ZT values of TE materials by nanotechnology. Currently, the highest ZT value ($ZT = 3.6$ at 580 K) was obtained in $PbSe_{0.98}Te_{0.02}$/PbTe quantum-dot superlattices (QDSLs) grown by molecular beam epitaxy (MBE), which was reported by Harman et al. [15] in 2005. Figure 2 shows the trends in both publications and patents on TE materials since 1965. It shows a blossoming in publications since 1995, and the publications from 2010 to 2013 are almost as numerous as those published within the previous 5 years (Fig. 2a), in which over 85 % are focused on inorganic TE materials, and only 15 % are about organic TE materials (Fig. 2b). Among all publications on inorganic TE materials, there are 32 % and 25 % of them are about silicon-based and oxide-based TE materials, respectively. Compared with publications, there are only about 450 patents on TE materials and related technology (Fig. 2c) since 1965, and most patents were filed during 1995–2010.

With the soaring interests in TE materials, there are many good reviews on the different types [16–22], including oxide based [16], organic based [17], and so on. For examples, as early as in 1986, Rowe [18] published a review on different kinds of potential TE materials; in 2009, Sootsman et al. [19] also summarized TE materials in different kinds; Chen and co-workers [20] have reviewed the progress on nanocomposite TE materials, and Li et al. [21] have highlighted the potential application of semiconductor nanowires in TEs, including the colloidal

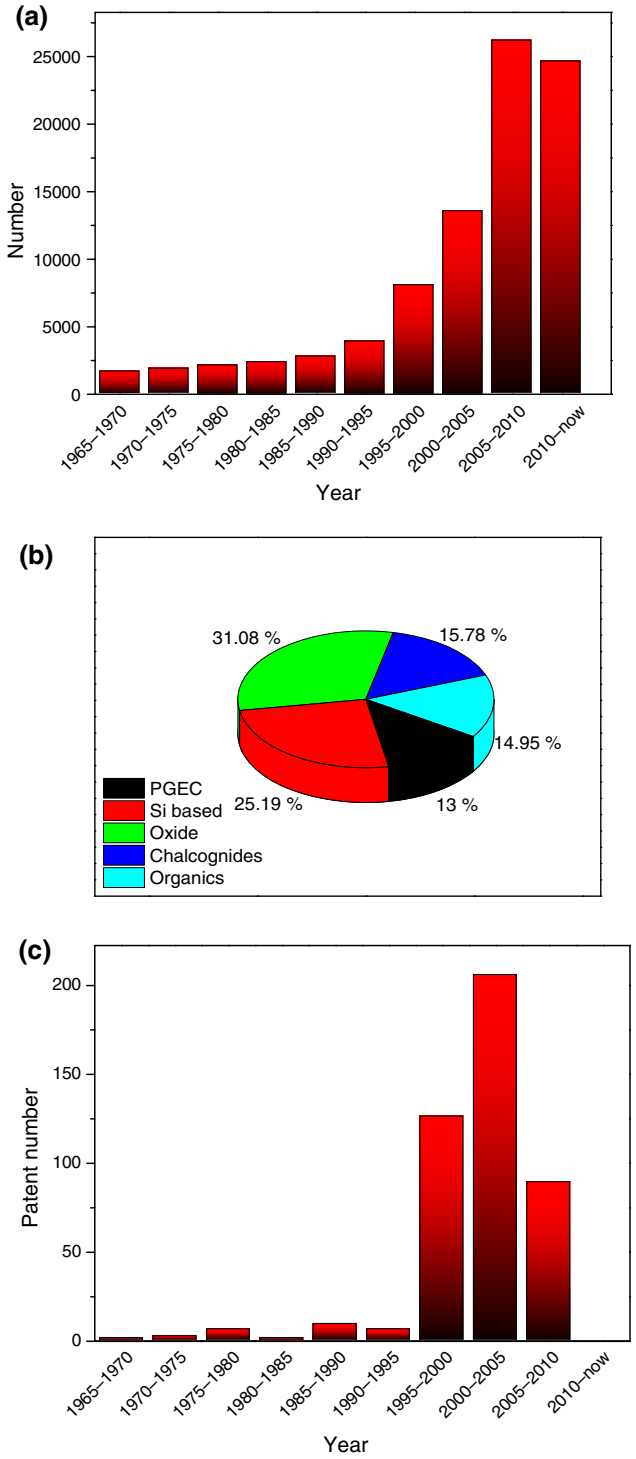

Fig. 2 (Color online) **a** Publications in the area of TE materials and related technology from 1965 to 2013; **b** Publications on different types of TE materials from 2010 to 2013; **c** Patents in the area of TE materials and related technology from 1965 to 2013. The data were collected from Science Direct data library by using "TE" as the key word

nanowires synthesized from wet chemistry [22–27]. On the basis of previous reviews, we summarize the latest progress for all the different types of TE materials in the past several years. We also show our perspectives on the future of TE materials and TE technology.

2 Recent progress in inorganic TE materials

There are many kinds of TE materials, from semiconductors to ceramics, from oxides to organics, from bulk to superlattice, and from nanoparticles to nanowires [16–27].

Figure 3 shows the application temperature ranges of different TE materials and the natural abundance of the relevant elements. Most state-of-the-art high-performance TE materials contain some toxic or low abundance elements. Here, we want to address the scientific progress made in different kinds of TE materials rather than their cost, toxicity, and effects on the environment during actual application.

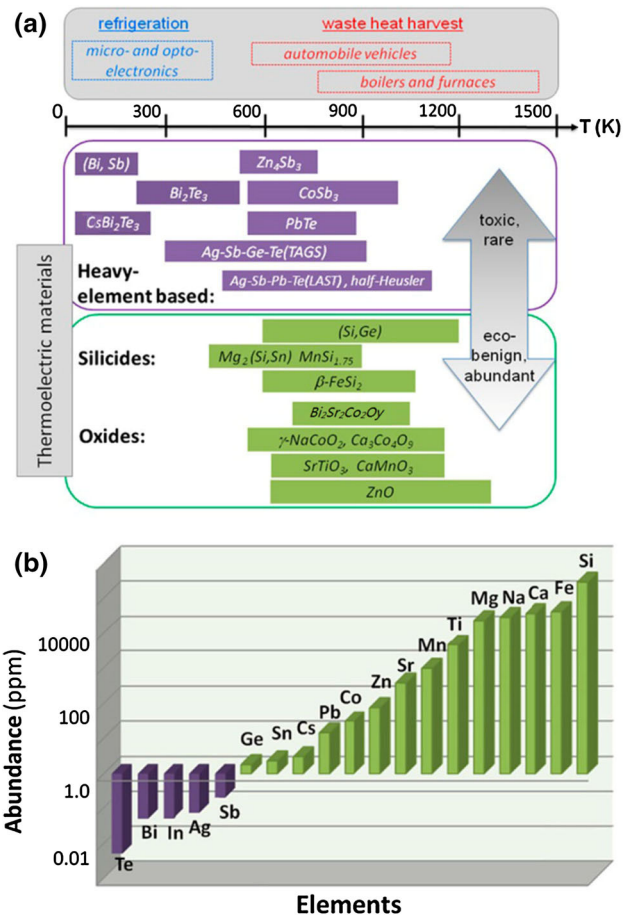

Fig. 3 (Color online) **a** Application temperature ranges of different kinds of TE materials; and **b** abundance of elements in the Earth's crust that is used in TE materials. Reprinted with permission from [16] Copyright 2011, Cambridge University Press

2.1 Metal chalcogenides

Metal chalcogenides have been extensively applied in many energy conversion and storage devices, such as solar cells, lithium ion batteries, fuel cells, supercapacitors, and TE generators and coolers [28–33]. In fact, metal chalcogenides, such as lead and bismuth-based selenides, and tellurides are prime candidates for TE applications due to their better and reliable performance in comparison with other TE materials. Their TE modules have been successfully commercialized with a *ZT* of around 1 [34]. Recently, their *ZT* values have been drastically improved to new records in the laboratory through nanotechnology, chemical doping, and engineering of their electronical structure. Some *ZT* values are above 2 or even 3 [35–38]. These breakthroughs and advances will be discussed in the following sections.

2.1.1 Lead chalcogenides

Lead is one of the most useful elements in good TE materials, as it has great natural abundance in the Earth's crust and can be easily processed. More importantly, it possesses a heavy atomic weight, which has benefits for the reduction of lattice vibration and thermal conductivity. Lead chalcogenides have been playing a dominant role in TE power generation for more than 50 years. Harman et al. [15] reported PbTe/PbTeSe quantum-dot superlattices with a *ZT* of 3.0 at 550 K. Although PbTe has been well investigated and synthesized by all kinds of methods, the *ZT* of bulk PbTe has been underestimated for a long time due to the difficulty in precisely measuring its thermal conductivity at high temperature until 2006, when the Snyder and co-workes [39] at the California Institute of Technology carefully studied the thermal conductivity of PbTe using an advanced laser flash technique. They corrected the *ZT* of p-type Na-doped PbTe and n-type I-doped PbTe from 0.8 and 0.7 to 1.5 and 1.4 at 750 K, respectively [39–41].

Another important advance was the use of nano-inclusions to reduce the thermal conductivity of PbTe [42–49]. The nano-inclusions usually come from a well-dispersed second phase and can be divided into "coherent" precipitates, which are slightly mismatched with the matrix, and "incoherent" precipitates, which show a clear boundary with the host. Both kinds of nano-inclusions can significantly reduce the thermal conductivity of PbTe-based TE materials, but they work by different mechanisms and show different effects. The coherent nano-inclusions act as point defects and scatter short wavelength phonons due to their slight mismatch with the matrix. Since the incoherent ones possess a large mismatch with the matrix, they work as nanoparticles and selectively scatter mid to long wavelength phonons. A *ZT* of 1.7–1.8 for both n-type and p-type PbTe has been realized through the use of coherent nano-inclusions of $AgSbTe_2$ [43], $NaSbTe_2$ [44], and SrTe [45]. While a *ZT* of 1.4–1.5 has been achieved in n-type PbTe by incoherent nano-inclusions of Sb and Ag_2Te [46, 47], it is slightly lower than that obtained by using coherent nano-inclusions due to their adverse effects on charge carrier mobility.

By improving phonon scattering on all relevant length scales in a hierarchical system (i.e., from atomic-scale lattice disorder and nanoscale-endotaxial precipitates to mesoscale grain boundaries), Kanishka et al. [50] achieved the maximum reduction in the lattice thermal conductivity and a *ZT* of 2.2 at 915 K in p-type PbTe doped with 4 % SrTe (molar concentration). Figure 4 shows the maximum *ZT* values for all length scales of scattering centers: the atomic scale (alloy scattering, dopant), the nanoscale (SrTe nanocrystals) to the mesoscale (grain-boundary scattering). By combining the effects of atomic-scale alloy doping, endotaxial nanostructuring, and mesoscale grain-boundary control, maximum phonon scattering can be achieved at high temperature, and the *ZT* can be increased beyond the values obtained from nanostructures alone. Use of multi-scale phonon scattering is a new strategy to minimize the thermal conductivity of TE materials.

Besides the conventional route of reducing thermal conductivity, enhancement of the power factor ($S^2\sigma$) has also been achieved by chemical doping. Biswas et al. [45] found that doping Se into p-type PbTe can increase carrier mobility without decreasing carrier concentration due to the convergence of electronic bands. Finally, they obtained a *ZT* of 1.8 in $Na_{0.02}Pb_{0.98}Te_{0.85}Se_{0.15}$.

In addition to lead chalcogenide nanocomposites made by solid-state reaction, there are more and more reports on nanostructured TEs made from wet-chemical approaches. For instance, Ibanez et al. [51] synthesized core–shell PbTe@PbS nanoparticles in organic solvent using a hot injection method. They tested the TE properties of the resultant nanoparticles after consolidating them into a pellet and obtained a *ZT* of 1.07 at 700 K. The high *ZT* of core–shell PbTe@PbS nanoparticles is because: (1) The

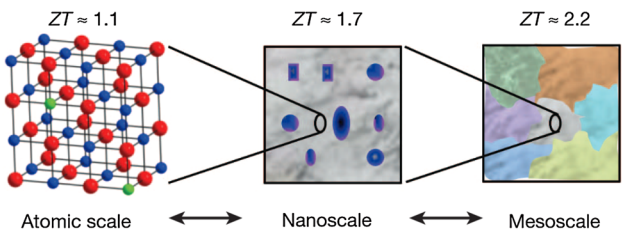

Fig. 4 (Color online) All-length-scale hierarchy in TE materials. Reprinted with permission from [50]. Copyright 2012, Nature Publishing Group

PbTe core functions like a p-type semiconductor, while the PbS shell acts as an n-type one, so that the compensation of the two kinds of charge carriers makes the electrical conductivity and the Seebeck coefficient relatively lower than those of pure PbTe and PbS at low temperature. With increasing temperature, however, the energy-activated charge carrier mobility is greatly enhanced and finally leads to an electrical conductivity that is one order of magnitude higher than those of pure PbTe or PbS. (2) The thermal conductivity is greatly reduced, not only by nanoscale effects and the lattice mismatch between PbTe and PbS, but also by partial alloying of PbS and PbTe, which can introduce a high density of point defects.

The other lead chalcogenides apart from PbTe, such as PbSe and PbS, have a similar structure to PbTe and a slightly larger band gap. Se and S are cheaper and less toxic than Te, and there are more opportunities to explore PbSe and PbS as alternatives. It was predicted that p-type PbSe would be a good TE material too [52]. This prediction was recently confirmed by Wang et al. [53], who doped PbSe with Na and got a *ZT* of 1.2 at 850 K. Zhang et al. [54] also doped PbSe with Al to obtain n-type PbSe with a high *ZT* of 1.3 at 850 K. In contrast to PbSe, only a moderate *ZT* of 0.8 at 900 K was obtained in PbS, even though some PbTe nano-precipitates were introduced into it [55].

2.1.2 *Bismuth chalcogenides*

Since their discovery in the 1950s, Bi_2Te_3 and its alloys with Sb and Se, with a *ZT* of 0.6 at 300 K, have been commercialized and used in TE refrigerators. Advances in nanotechnology have recently boosted the *ZT* of this conventional TE material to a new record, as demonstrated by a *ZT* of 2.4 at 300 K obtained from a superlattice of Bi_2Te_3–Sb_2Te_3 films in 2000 [56]. This breakthrough not only demonstrates how nanoscale effects can improve the performance of conventional TE materials but also has led to a burst of research on TE nanomaterials.

Similar to lead chalcogenides, the introduction of nanostructures into the bismuth chalcogenide matrix can improve its TE performance. Chen and co-workers [57] and Xie et al. [58] increased the *ZT* of p-type $Bi_xSb_{2-x}Te_3$ from 1 to 1.4–1.5 by employing nano-inclusions during powder metallurgy synthesis. The same process did not work for n-type $Bi_2Te_{3-x}Se_3$, because the high carrier concentration decreases the average carrier mobility, and it increases the thermal conductivity. Another reason lies in the formation of Te vacancies during the ball-milling process, which affects the electrical conductivity.

The use of different well-dispersed particles to simultaneously enhance the phonon scattering, and the Seebeck coefficient can improve the *ZT* of Bi_2Te_3-based TE materials. Liu et al. [59] achieved a *ZT* of 0.94–0.99 in n-type $Cu_{0.01}Bi_2Te_{2.7}Se_{0.3}$, which is higher than that of $Bi_2Te_{2.7}Se_{0.3}$ ($ZT = 0.85$). Besides the reduction of thermal conductivity resulting from nano-inclusions, Ko et al. [60] also observed an increase in the Seebeck coefficient due to a carrier-selective scattering effect in Pt-doped Sb_2Te_3. Liu et al. [61] investigated the effect of SiC on the transport properties of n-type and p-type Bi_2Te_3 and found a selective carrier scattering effect caused by the SiC particles. Ren and co-workers [62] successfully increased the *ZT* of n-type $Bi_2Te_{2.7}Se_{0.3}$ to 1.04 by improving its electrical conductivity through the reorientation of the *ab*-planes of small crystals during multiple-step hot pressing of ball-milled nanopowders.

In 2010, Ferdows and Roger [63] theoretically calculated the *ZT* of Bi_2Te_3 thin films (five atomic layers thick) to be as high as 7.2 at room temperature. The high *ZT* results from the change in the distribution of the valence band density due to the quantum confinement in the thin film. There is no experimental result supporting this calculation, however. In addition to thin films, the *ZT* of Bi_2Te_3 nanowires has also been theoretically calculated, and the results show a strong diameter dependence, e.g., the *ZT* value can be over 6 if the nanowire diameter is smaller than 5 nm. Inspired by the high *ZT* of nanowires from theoretical predictions, Zhang et al. [64] synthesized uniform 8-nm Bi_2Te_3 nanowires and achieved a *ZT* of 0.96 at 380 K. The authors also designed Bi_2Te_3 nanowire-based heterostructures, such as Te@Bi_2Te_3, Bi_2Te_3@PbTe, although the *ZT* of the Te@Bi_2Te_3 heterostructure was only around 0.23 at 400 K. This value was two times higher than that of pure Te nanowires, but much lower than that of pure Bi_2Te_3 nanowire (0.96 at 380 K) [65].

Besides the use of zero-dimensional nanoparticles or one-dimensional (1D) nanowires to improve their TE performance, introduction of two-dimensional (2D) nanosheets into bismuth chalcogenides can also lead to a high *ZT*. Li et al. [66] mixed graphene with Bi_2Te_3 to improve its conductivity, resulting in a 1.5 times higher *ZT* (0.3 at 350 K) for the composites than for single crystal Bi_2Te_3. Although the *ZT* value is low, their work provides an idea to prepare hybrid TE composites with enhanced performance.

2.2 Superionic conductors

An ideal TE material should be a phonon glass and an electron crystal (PGEC), which can simultaneously exhibit high electrical conductivity and low thermal conductivity, and thus show high *ZT*. Some superionic conductors such as cuprous and silver chalcogenides have similar properties. In contrast to the structure of lead and bismuth chalcogenides, cuprous and silver chalcogenides have a

special structure where the chalcogen anions form a crystalline lattice and provide a pathway for charge carriers, while the cuprous or silver cations (i.e., Cu^+ and Ag^+) are highly disordered around the chalcogen sublattice at high temperature. Cu^+ or Ag^+ ions can move fast like liquid at high temperature, which leads to extremely low thermal conductivity. The liquid-like behavior of Cu^+ and Ag^+ makes their chalcogenides phonon liquid and electron crystal (PLEC), essentially similar to PGEC. Therefore, they exhibit outstanding TE performance, demonstrated by the *ZT* of p-type $Cu_{2-x}Se$ (1.6 at 1,000 K), the highest value among all bulk TE materials [67]. In 2013, Liu et al. [68] got an even higher *ZT* (2.3 at 400 K) in n-type Cu_2Se. This specific high *ZT* was obtained by the critical scattering of electrons and phonons during the second-order phase transition in Cu_2Se. The temperature fluctuation near phase transition temperature can lead to the "critical scattering", which can selectively scatter phonons without influence on electrons. This offered a new strategy to get a high *ZT* at phase transition temperature.

Figure 5 shows the structure of cuprous selenide. The Se atoms form a rigid face-centered cubic lattice, and the Cu^+ ions are highly disordered around the Se sublattice.

It should be noted that the copper and chalcogen can form various compounds with complicated structures. Figure 6 is the binary Cu–Se phase diagram, clearly showing the variation of crystal phases and compositions that can occur with increasing temperature and ratio of elements. Nevertheless, there are few compounds (e.g., Cu_2Se or $Cu_{2-x}Se$) that are suitable for TE application.

The low thermal conductivity of cuprous and silver chalcogenides is attributed to the liquid-like behavior of Cu^+ or Ag^+, which is due to their fast movement arising from the crystal phase transition. Their high electrical conductivity is due to the deficiency of Cu^+ or Ag^+. As cuprous and silver chalcogenide nanostructures have smaller size and higher surface to volume ratio than their bulk analogs, they have a higher degree of deficiency and disorder and are expected to show better performance. Although different copper and silver chalcogenide nanostructures have been synthesized in different ways [69–72], there are only few reports on their TE properties due to difficulties in large-scale preparation of their nanostructures with well-defined compositions and crystal structures, as well as uniform size and morphology. Recently, Xiao et al. [73] synthesized monodispersed Ag_2S, Ag_2Se, and Ag_4SeS nanocrystals through a solvothermal method and then investigated the TE properties of these nanocrystals, especially at the phase transition temperature. Their *ZT* at the corresponding transition temperature is in an order of ZT_{Ag4SeS} (0.33) > ZT_{Ag2Se} (0.23) > ZT_{AgS} (0.12). Later on, the authors successfully doped Ag_2Se nanocrystals with Bi^{3+} to switch the conductivity from p-type into n-type, and they obtained a *ZT* of 1.5 at 700 K [74]. Compared with silver chalcogenide nanostructures, there is much less reports on the TE properties of copper chalcogenide nanomaterials. Zhang et al. [75] prepared $Cu_{2-x}Se$ nanowires by a hydrothermal method in the Teflon-lined autoclaves and measured their Seebeck coefficient to be 180 μV/K. Unfortunately, there is nothing about the *ZT* value of these nanowires.

The above research suggests that superionic conductors could be high-performance TE materials, especially in nanostructured form. There is considerable scope for investigating the TE application of cationic and anionic superionic conductors.

2.3 Metal oxides

Metal oxide-based TE materials have several advantages in comparison with metal chalcogenides. First, they possess good chemical and thermal stability, and thus can be used in a large temperature gradient in air. Second, they are environmentally friendly and cost-effective. Third, they could exhibit novel non-linear, non-local TE effects (i.e., the Benedicks effect) induced by a large temperature gradient, which may be thermoelectrically favorable [76, 77]. Fourth, their TE performance can be tuned over a wide

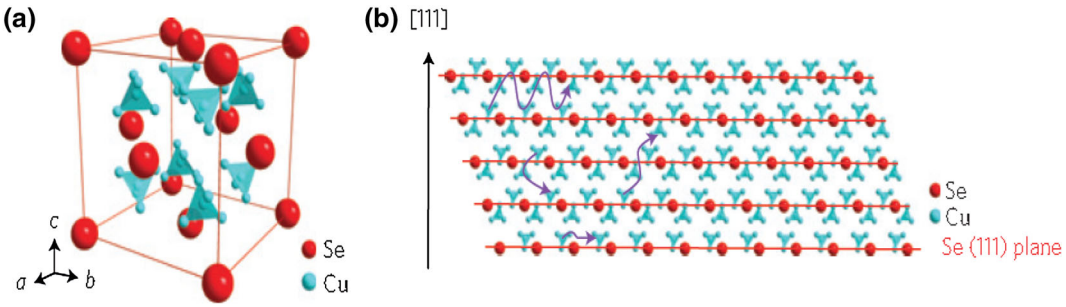

Fig. 5 (Color online) Crystal structure of β-Cu_2Se with a cubic anti-fluorite structure: **a** unit cell; **b** projected plane along the cubic [110] direction. The arrows indicate that the Cu ions can freely travel among the interstitial sites. Reprinted with permission from [67]. Copyright 2012, Nature Publishing Group

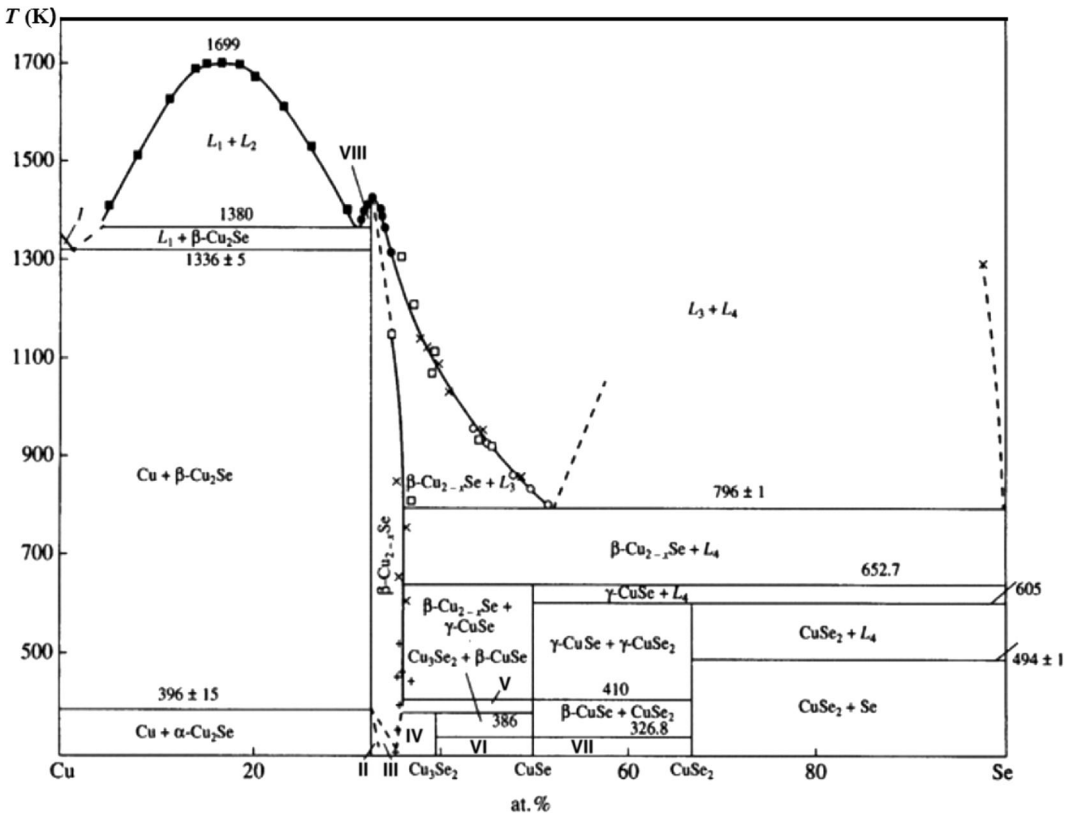

Fig. 6 Phase diagram of Cu–Se system. Phase (I) Cu+L_1, (II) α-$Cu_{2-x}Se$, (III) α-$Cu_{2-x}Se$+β-$Cu_{2-x}Se$, (IV) β-$Cu_{2-x}Se$+Cu_3Se_2, (V) β-$Cu_{2-x}Se$+β-CuSe, (VI) Cu_3Se_2+α-CuSe, (VII) α-CuSe+$CuSe_2$, and (VIII) L_2+β-Cu_2Se. Reprinted with permission from [67]. Copyright 2012, Nature Publishing Group

range by engineering their structure and composition. In addition, they can be also used in other energy conversion devices (e.g., solar cells and lithium ion batteries), which could improve the performance of these devices.

Despite the above advantages, oxide-based TE materials have lower *ZT* compared with conventional TE materials such as Bi_2Te_3 due to their relatively higher thermal conductivity. There are several types of TE oxides, including cobalt oxides (p-type), manganese oxides (n-type), and zinc oxides (n-type semiconductors). In 1997, research interest in oxide-based TE materials was ignited when p-type Na_xCoO_2 with a *ZT* around 1 was discovered. Since then, some layered oxide materials have been predicted to show a reasonably high *ZT* if different kinds of layers (unit nanoblocks) with different compositions, and symmetries are integrated into hybrid crystals or superlattices, in which each layer can play its own role in realizing independent control of electrons and phonons.

The oxide layer structure can be strongly influenced by the processing method that is used. Noudem et al. [78] investigated the effect of spark plasma sintering (SPS) on the morphology of $Ca_{0.95}Sm_{0.05}MnO_3$ and its TE performance. They got a higher power factor than in previous reports by optimizing the sintering parameters. Inspired by these findings and the fact that nanostructures can effectively decrease thermal conductivity, investigations on layered oxide-based TE materials have rapidly increased and made great progress. He et al. [16] have summarized the progress achieved in oxide-based TE materials from 2000 to 2010. Figure 7 displays some representative oxide TE materials investigated in this period. Since now, the highest *ZT* obtained in oxides was around 2.4 at room temperature which was realized on $SrTiO_3$ superlattice [79].

In 2011, Jood et al. [80] successfully doped Al into ZnO nanoparticles using a microwave solvothermal approach (Fig. 8). The resultant doped ZnO nanoparticles showed a *ZT* of 0.44 at 1,000 K, 50 % higher than that of the best non-nanostructured counterpart at the same temperature. Their work again proved the effectiveness of nano-inclusions in decreasing thermal conductivity.

In addition to ZnO, BiCuSeO was also found to be a potential candidate as an oxide-based TE material by Li et al. [81] in 2012. A *ZT* of 0.7 was obtained in this material at 773 K. This oxide not only possessed good electrical conductivity and a large Seebeck coefficient, but also showed extremely low thermal conductivity due to its low speed of sound and Young's modulus. In addition, by

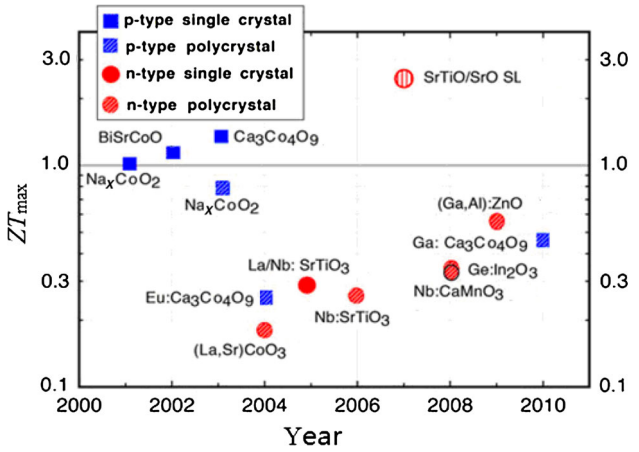

Fig. 7 (Color online) Maximum figure of merit values of p-type and n-type TE oxides from 2000 to 2010. Reprinted with permission from [16]. Copyright 2011, Cambridge University Press

purifying the constitutive phase and reducing grain size, the electrical conductivity could be significantly enhanced while maintaining a large Seebeck coefficient. Later, Li et al. [82] reported a higher *ZT* value of 1.1 at 923 K for $Bi_{0.875}Ba_{0.125}CuSeO$. This high *ZT* value was achieved by the combined effect of heavy doping with Ba and refinement of grain size (200–400 nm). Guided by the previously existing TE phases, Constantinescu et al. [83] used the phase diagram equilibrium to design new thermoelectric TE oxides based on other transition metals. They synthesized cobalt-free $BaFeO_x$ which has the same perovskite structure as Na_xCoO_2. Although the obtained power factor is too low for practical applications, their work provides an idea for designing new TE materials, due to the higher abundance and lower toxicity of Ba, Fe in comparison with cobalt, lead, bismuth, and the other heavy elements used in conventional TE materials.

Although there are many investigations on the TE properties of oxide materials, the development of nanotechnology and doping techniques would provide new opportunity for them. Their *ZT* values would be drastically improved in near future, and they would become more competitive than other TE materials, because they have high thermal and chemical stability, in addition to their low fabrication cost.

2.4 Silicon-based materials

Silicon is cheap, environmentally friendly, and has been widely used in semiconductor devices and solar cells. Bulk silicon was proved not a good TE material, as it has high thermal conductivity (around 150 W/(m K)). This drawback has been successfully overcome by reducing its grain size down to nanoscale dimensions. Recently, a *ZT* of 0.6 at room temperature was achieved in B-doped Si nanowires (50 nm in diameter) which were fabricated by etching silicon wafers [84]. Akram et al. [85] also reported the efficient TE performance of silicon nanowires with cross-sectional areas of 10 nm × 20 nm and 20 nm × 20 nm. A *ZT* of 1 at 200 K was achieved by varying the nanowire diameter from 10 to 20 nm and by varying the impurity doping level. In addition to nanowires, Sabah et al. [86] employed a simple high energy ball-milling method to synthesize doped Si nanoparticles on a large scale and then consolidate them into pellets. A *ZT* of 0.7 at 1,275 K was measured for this n-type bulk nanostructured Si, which is 3.5 times larger than that of heavily doped single-crystal Si.

Besides experimental research, theoretical investigations on the TE properties of nanoscale Si have been carried out in parallel. Lee et al. [87] computed the room temperature TE properties of nanoporous silicon using a combination of classical molecular dynamics for the lattice thermal conductivity and ab initio density functional theory for the electrical conductivity, Seebeck coefficient, and electronic contribution to the thermal conductivity. They predicted that the *ZT* could increase by 2 orders of magnitude over

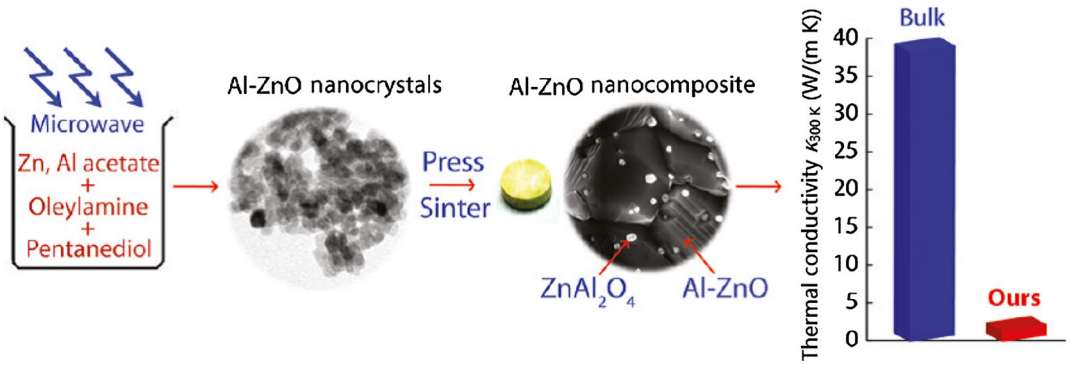

Fig. 8 (Color online) Schematic illustration of the fabrication of Al containing ZnO nanocomposites with low thermal conductivity, obtained by the cold-pressing and sintering of Al-doped ZnO nanocrystals synthesized by the microwave-stimulated solvothermal method. Reprinted with permission from [80]. Copyright 2011, American Chemistry Society

that of the bulk due to the combination of the nanometer size pores, which can greatly reduce the thermal conductivity, and the ordered arrangement of pores which allows for only a moderate reduction in the power factor. Yang et al. [88] calculated the lattice thermal conductivity of nanocrystalline, nanoporous, and superlattice Si. The results show that (1) the lattice thermal conductivity can be remarkably reduced through the boundary scattering effect and intrinsic size effect in these nanomaterials; (2) nanoporous Si exhibits smaller lattice thermal conductivity than Si nanowires due to the porosity effect; (3) fully dense Si nanocomposites have comparable lattice thermal conductivity to that of Si nanowires; and (4) periodic quantum structures, such as superlattices, are not necessary for the reduction of thermal conductivity.

Silicon nanostructures have a bright prospect in TE applications, as they can be easily fabricated using the existing semiconducting industry. Their TE device can be easily combined with electronic devices. More importantly, their TE performance can be significantly improved by doping with germanium, although it is very expensive. How to improve their *ZT* without use of expensive elements would be an important subject in this area. Here, we want to address two important types of silicon-based TE materials (i.e., SiGe and Mg_2Si) in detail in the following section.

2.4.1 *SiGe-based TE materials*

The addition of germanium into the silicon matrix can effectively reduce the lattice thermal conductivity. The SiGe alloys that are thus formed are currently the best TE materials at high temperature (around 1,000 °C) and are therefore used in radioisotope TE generators (RTG) and some other high temperature applications. For example, SiGe TE modules with a material ZT of 0.5 (p-type) and 0.9 (n-type) have been used in RTGs by NASA in the United States since 1976 [88].

Recently, a pronounced enhancement in *ZT* values has been demonstrated for both n- and p-type SiGe alloys by using them in nanostructured form, which can increase the phonon scattering [89–91]. One example is that the thermal conductivity was greatly reduced, and the maximum *ZT* of p-type nanostructured $Si_{80}Ge_{20}B_5$ was improved from 0.5 to 0.95 [89], while the *ZT* of n-type $Si_{80}Ge_{20}P_2$ was increased from 0.93 to around 1.3 [90]. The concentration of Ge is still too high, however, leading to high fabrication cost. It should be noted that omitting the Ge would lead to a drop in *ZT* value. In 2009, Zhu et al. [92] added 5 % Ge into GaP and P co-doped Si to achieve a *ZT* of 0.94 at 900 °C. Yu et al. [93] also achieved a *ZT* of 1.3 at 900 °C for nanocomposites of $(Si_{95}Ge_5)_{0.65}(Si_{70}Ge_{30}P_3)_{0.35}$ by using a modulation doping method. The mechanism of modulation doping is shown in Fig. 9. The dopants (P) in

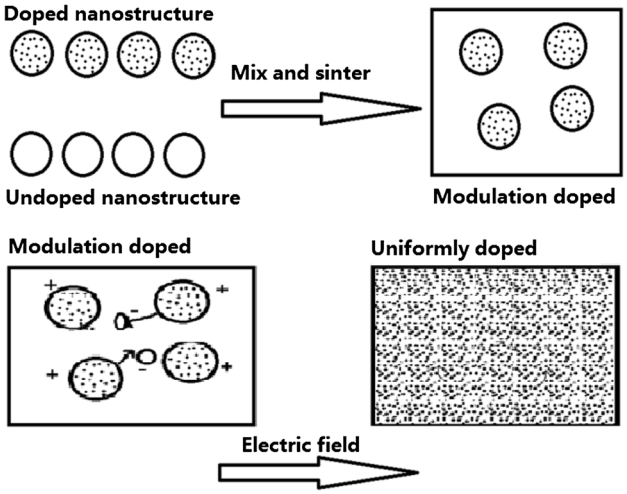

Fig. 9 Schematic diagram of modulation doping and uniform doping

the nanoparticles of $Si_{70}Ge_{30}$ offer extra charge carriers, while the scattering between the charge carriers and the ionized dopants is greatly reduced, as the dopants are localized in the nanoparticles. Hence, the power factor is greatly enhanced. Their work provides a new approach to increase the concentration of charge carriers while reducing the loss of mobility.

In 2009, Mingo et al. [94] proposed a "nanoparticle-in-alloy" approach to enhance the TE performance of SiGe. With nanosized silicide and germanide fillers in the SiGe matrix, a fivefold increase in the *ZT* at room temperature and a 2.5 times increase at 900 K were achieved. They also predicted that there must be an optimal nanosize that can minimize the nanocomposite's thermal conductivity. Meanwhile, the nanoparticles do not impair the electrical conductivity because of size control. Finally, a *ZT* of 1.7 at 900 K was obtained through this approach.

In 2012, a *ZT* of 2 at 800 K was reported by Lee et al. [95] who simultaneously tested the thermal conductivity, electrical conductivity, and power factor of a single SiGe nanowire. The high *ZT* arises from the huge reduction in thermal conductivity due to the quantum confinement effect. This result demonstrates the great potential of nanostructured SiGe-based TE materials.

2.4.2 *Mg_2Si-based TE materials*

Despite the high performance of SiGe-based TE materials, the use of Ge results in high cost. Alternative TE materials could be Mg_2B_{IV} (B_{IV} = Si, Ge, and Sn) compounds and their alloys, among which, Mg_2Si-based materials have been extensively investigated, as they can be used in the engine operating temperature range (i.e., 500–800 K). More importantly, they have lower density, higher resistance to oxygen, non-toxicity, and environmental friendliness in

comparison with other TE materials used in the same temperature range, such as $CoSb_3$ and PbTe [96, 97]. The huge abundance of Mg and Si [98–100] leads to low fabrication cost, which would enable their wide application.

Mg_2Si is an intermetallic compound or Zintl salt with a high melting point and metallic luster at room temperature. It is a poor n-type semiconductor and sensitive to water. Vining et al. [101] proposed that Mg_2Si could possess a higher *ZT* due to the fact that the material factor ($\beta = (T/300)(m^*/m_e)^{3/2}$) of Mg_2Si (14) is much larger than those of SiGe (1.2–2.6) and $FeSi_2$ (0.05–0.8). Later experiments proved that the *ZT* of intrinsic Mg_2Si is relatively low, i.e., smaller than 0.2 [102–106]. The reason for the low *ZT* is its high thermal conductivity due to the light weight of the Si atoms. Another drawback of this material is the difficulty in preparing highly pure Mg_2Si due to the similar properties of Mg and Si. The boiling point of Mg (1,380 K) is the same as the melting point of Mg_2Si (1,380 K). In addition, Mg and Si have poor solubility in each other and very different vapor pressures. The separation of elements usually leads to a degradation of performance during the application of Mg_2Si as a TE material.

There are mainly three routes to improve the *ZT* of Mg_2Si: (1) doping with various elements such as Al, Sb, Bi, and Na; (2) formation of a homogeneous solid solution of $Mg_2Si_{1-x}Sn_x$ and $Mg_2Si_{1-x}Ge_x$; and (3) the use of nanostructures. Nikhil et al. [107] investigated the effect of crystallite size on the TE properties of nanoscale Mg_2Si. They thought that nanostructure in Mg_2Si may not be effective to increase *ZT* because of the detrimental loss of carrier mobility at the grain boundaries, but Yang et al. [108, 109] reported that the *ZT* of nano-Mg_2Si can be increased to 0.36 at 811 K by the use of mechanical alloying and SPS methods. They further increased the *ZT* to 0.8 at 823 K by doping nano-Mg_2Si with Bi. Using a similar strategy, Zaitsev et al. [110] doped $Mg_2Si_{0.4}Sn_{0.6}$ with Sb and got a *ZT* of 1.1 at 780 K. Noda et al. [111] doped $Mg_2Si_{0.6}Ge_{0.4}$ with Sb and Ag, and achieved a *ZT* of 1.07 at 663 K for Sb-doped $Mg_2Si_{0.6}Ge_{0.4}$ and 1.68 at 629 K for its Ag-doped analog, respectively.

2.5 PGEC TE materials

One type of high performance bulk TE materials is the PGEC, as identified by Slack et al. [12], which can scatter most phonons to result in low thermal conductivity, as well as conducting electrons to promote high electrical conductivity, by forming a complex cage-like structure filled with heavy atoms. Skutterudites, clathrates, and half-Heusler alloys are such TE materials. They are mainly prepared by casting or powder metallurgic method, and their TE performance can be improved by chemical doping or substitution.

2.5.1 *Skutterudites*

As shown in Fig. 10, skutterudites are bulk TE materials with the structure of (Co, Ni, Fe)(P, Sb, As)$_3$ and cubic space group Im3. They contain vacancies into which low-coordination ions (usually rare earth elements) can be inserted to decrease the thermal conductivity by enhancing phonon scattering without reducing electrical conductivity. Such a structure makes them exhibit PGEC behavior. The chemical formula of skutterudites can be expressed as ReM_4X_{12}, where Re is a rare earth element, M is a transition metal element, and X is a nonmetal element from Group V, such as phosphorus, antimony, or arsenic. *ZT* of skutterudites can be significantly improved by double, triple, and multiple filling of elements into the vacancies in their structure. Usually, alkali metals, alkaline-earth metals, lanthanides, and similar elements are selected as "fillers" or "dopants" for skutterudites because of their moderate atom size. Hence, the selection and combination of different "fillers" is very crucial for achieving high TE performance. Replacement of host atoms in lattice sites, such as substitution for Co and Fe, has also been identified as an effective way to reduce thermal conductivity.

The merits of skutterudites include (1) the *ZT* is relatively high and can be easily tuned by controlling their compositions and structures; (2) components are relatively cheap and non-toxic; (3) the application temperature can be up to 600 °C. The sublimation of Group V elements (e.g., antimony), however, and poor resistance to oxidation limit their wide application, as oxidation and volatilization easily take place in harsh environments such as in air at high temperature, which lead to a rapid degradation of TE properties and shortens the lifetime of TE generators [112–118].

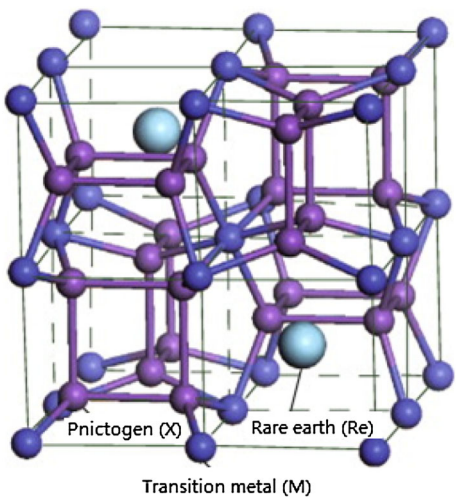

Fig. 10 (Color online) Crystal structure of skutterudites and element distribution in the unit cell

Recently, great progress has been achieved in improvement of the TE properties of skutterudites. In 2011, $CoSb_3$ with multiple fillers of Ba, La, and Yb were synthesized, and a high *ZT* of 1.7 at 850 K was realized [119]. The dependence of skutterudite TE properties on the filled fraction and a comparison of their *ZT* with those other TE materials are shown in Fig. 11.

In addition to the tuning with fillers, a *ZT* of 1.8 has been achieved in Sr-, Ba-, Yb-filled $CoSb_3$ by employing a high pressure torsion process, which can refine the grain size of the material via severe plastic deformation [120]. The refinement of grain size increases the amount of interfaces and leads to further reduction in thermal conductivity.

2.5.2 *Clathrates*

Compared with skutterudites, clathrates possess a more complex cage-like structure and a wider variation in composition. They have a general formula of $A_xB_yC_{46-y}$ (type I) and $A_xB_yC_{136-y}$ (type II), in which B and C are elements from Groups III and IV and can form a framework serving as host for "guest" atoms of element A (alkali or alkaline-earth metal), which are encapsulated between two different polyhedra. The structure of Type I clathrates is shown in Fig. 12. The yellow atoms denote the guest atoms, with the light yellow at the 6d position and the dark yellow at the 2a position. The host structure is also shown with varying color intensity: 6c (light blue), 16i (medium blue), and 24 k (dark blue). Figure 12a illustrates the unit cell with its large tetrakaidecahedral (24-atom) cage in blue and dodecahedral (20-atom) cage in red. Figure 12b depicts the bonding arrangements of the different host structure sites, where the atom size is intended to enhance the clarity. In Fig. 12c, the different guest atom sites in the large cage are illustrated: 12h (light red), 24j (medium red), and 24k (dark red). The main differences between types I and II clathrates are the number and size of the vacancies in their unit cells.

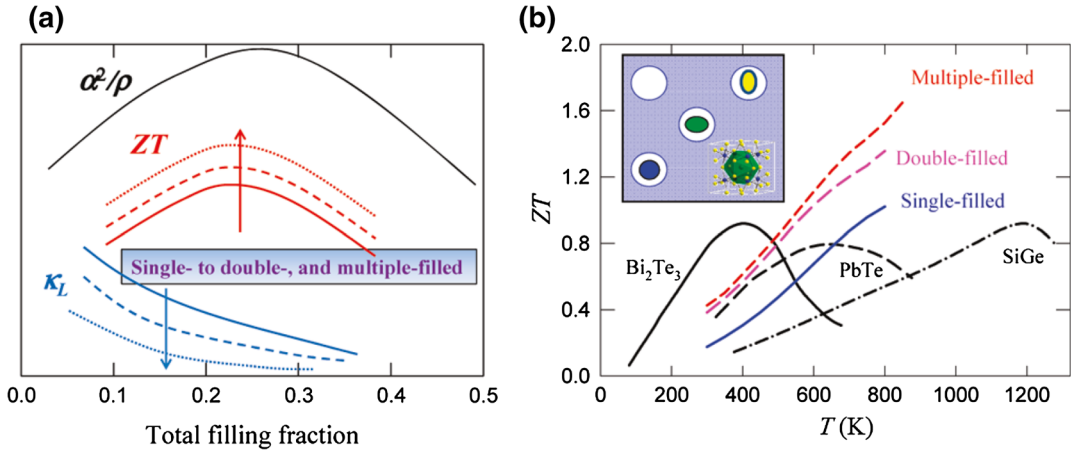

Fig. 11 Relationship between TE properties and the filled fraction of skutterudites (**a**) and comparison of *ZT* with other TE materials (**b**). α^2/ρ is power factor; κ_L is the lattice thermal conductivity. Reprinted with permission from [119]. Copyright 2011, American Chemical Society

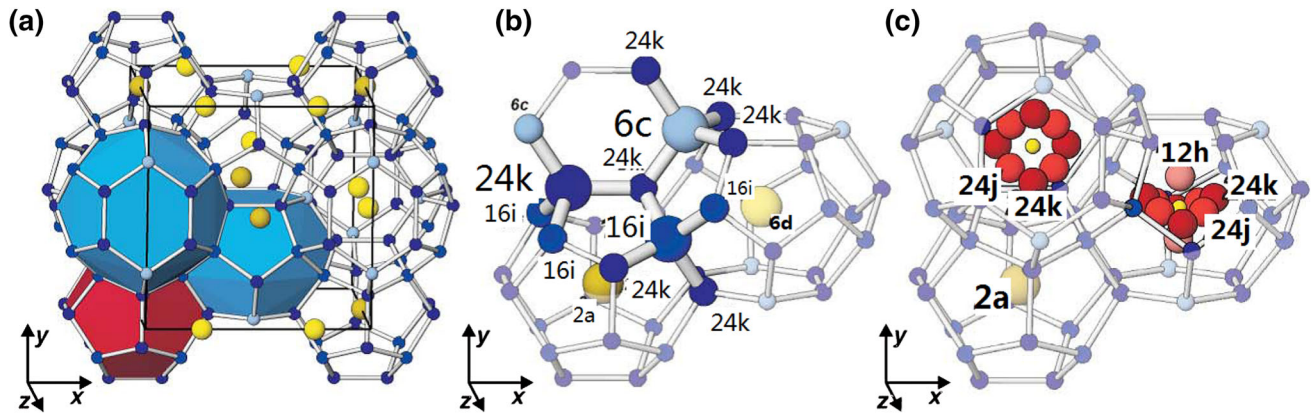

Fig. 12 Crystal structure of Type I clathrate (**a**) unit cell; (**b**) bonding arrangements of the different host structure sites; (**c**) different guest sites. Reprinted with permission from [121]. Copyright 2007, American Chemical Society

Their complex unit cells allow a significant reduction in the thermal conductivity and lead to a high *ZT*. Unlike skutterudites, both single crystals and polycrystalline powders of clathrates can have high *ZT* and can be tuned over a wide range. In addition, they are highly stable at high temperature, both chemically and thermally. They also show excellent compatibility with other devices in multimodal applications.

Powder metallurgical and crystal growth techniques have been well developed to synthesize clathrates. A direct approach to optimize the TE properties of semiconducting type I clathrates is substitutional doping, where some framework atoms are replaced by dopant atoms. Compared with type I clathrates, their type II analogs have not been intensively studied and would be an interesting subject, because a partial filling of their polyhedra allows a better tuning of their electrical properties and a better control of the dopant concentration. Some important progress in this area was reviewed by Christensen et al. [121].

The highest *ZT* of 1.35 at 900 K was reported in the n-type clathrate $Ba_8Ga_{16}Ge_{30}$ in 2006 [122]. Because they are limited by the "Zintl rule" [123–125], optimization of the power factors of stable clathrates is very difficult, and there are rare reports on the reduction of lattice thermal conductivity in clathrates by nano-engineering approaches [126]. Inspired by the successful use of high pressure torsion (HPT) on skutterudites, Yan et al. [127] tried to obtain a higher *ZT* for $Ba_8Cu_{3.66}Ge_{40.30}In_{1.65}$ by the same HPT method. Unfortunately, their results showed that compared with hot-pressed samples, the carrier concentration was reduced, and the increase in *ZT* was negligible, although a higher electrical resistivity and Seebeck coefficient were achieved after HPT processing.

2.5.3 *Half-Heusler alloys*

Half-Heusler alloys (ABX) have potential in high temperature power generation, especially as n-type material. These alloys have three components selected from different element groups or from the same group. A and X are transition metals, and B may be a metal or non-metal. The crystal structure of a half-Heusler alloy could be considered as a simple rock salt structure formed by A and X, which is filled with B at one of the two body diagonal positions (1/4, 1/4, 1/4) in the unit cell, leaving the other one (3/4, 3/4, 3/4) unoccupied [128]. Figure 13 shows the structure of a typical half-Heusler ABX alloy and the element sources of A, B, and X. The structure allows doping on each of the three occupied face-centered cubic (fcc) sublattices to tune the TE properties individually. These alloys are relatively cheap and have a flexible composition. Additionally, they have a promising *ZT* in the temperature range from 600 to 1,000 K.

Figure 14 shows the recent progress in both n-type and p-type half-Heusler alloys. In 2010, Yan et al. [129]

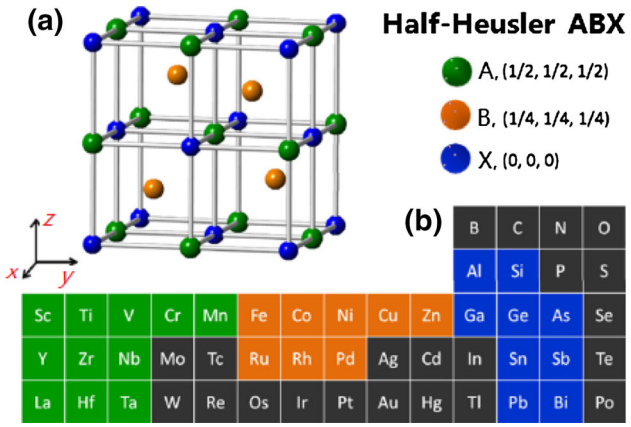

Fig. 13 (Color online) Structure of a typical Half-Heusler ABX alloy and the element sources of A, B, X. Reprinted with permission from Ref. [20]. Copyright 2012, Elsevier

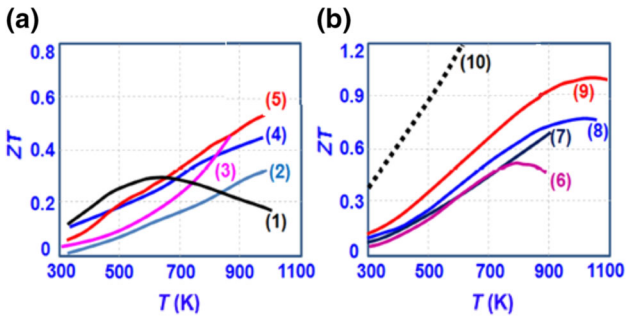

Fig. 14 (Color online) Overview of the most promising p- (**a**) and n-type (**b**) half-Heusler alloys. (1) $ErNi_{1-x}Pd_xSb$; (2) $ZrNi_{0.8}Ir_{0.2}Sn$; (3) $TiCo_{0.85}Fe_{0.15}Sb$; (4) $ZrCoSn_{0.1}Sb_{0.9}$; (5) $Zr_{0.5}Hf_{0.5}CoSb_{0.8}Sn_{0.2}$; (6) $Ti_{0.5}Zr_{0.25}Hf_{0.25}Co_{0.95}Ni_{0.05}Sb$; (7) $Ti_{0.6}Hf_{0.4}Co_{0.87}Ni_{0.13}Sb$; (8) $Zr_{0.75}Hf_{0.25}NiSn_{0.975}Sb_{0.025}$; (9) $Zr_{0.4}Hf_{0.6}NiSn_{0.98}Sb_{0.02}$; (10) $Zr_{0.25}Hf_{0.25}Ti_{0.5}NiSn_{0.998}Sb_{0.002}$. Reprinted with permission from [131]. Copyright 2012, MDPI

reported p-type $Zr_{0.5}Hf_{0.5}CoSb_{0.8}Sn_{0.2}$ with a *ZT* of 0.8 at 973 K. The *ZT* enhancement comes from a simultaneous increase in the Seebeck coefficient and a decrease in the thermal conductivity due to nanostructures. The samples were made in three steps: (1) preparation of alloyed ingots using the arc melting method; (2) ball milling of the resultant ingots into nanopowders; and (3) preparation of a dense bulk by hot pressing of nanopowders.

One common approach to enhancing TE performance is partial replacement of elements by their neighbors from the same group or the same row to form nano-inclusions. Benjamin et al. [130] substituted one neighboring atom with fewer valence electrons and one with more electrons. The amounts of the fillers or dopants were adjusted so that the deficiency and excess electrons were compensated. Therefore, the amount of valence electrons was not changed, and the semiconducting properties were retained. They obtained a solid solution of $TiCo_x(Ni_{0.5}Fe_{0.5})_{1-x}Sb$, in which Co was substituted equally by Fe and Ni, and *ZT* was

enhanced by a factor of about seven to a value of 0.04 at 400 K for $TiCo_{0.8}(Ni_{0.1}Fe_{0.1})Sb$ due to the reduction in the thermal conductivity and the retention of a high Seebeck coefficient. Although the *ZT* value is still relatively low, their work demonstrates a new way of substitution: the use of one neighboring atom with fewer valence electrons and one with more electrons to improve the *ZT* of half-Heusler alloys. More progress in nanostructured half-Heusler materials has been summarized in [131].

3 Organic TE materials

As described above, the advances in the engineering of inorganic nanostructures have resulted in notable improvement in *ZT*. Nevertheless, inorganic TE materials have issues of either high fabrication cost or toxicity. The conducting-polymer-based TE materials offer a new solution with low cost and environmental friendliness. Figure 15 shows the chemical structures of some conducting polymers. The conducting polymers usually have backbones of contiguous sp^2 hybridized carbon centers. One valence electron on each center resides in a p_z orbital, which is orthogonal to the other three sigma-bonds. p_z orbitals conjugate with each other to form delocalized orbitals. In principle, these materials can be doped by reduction, which adds electrons to unfilled bands. Undoped conjugated polymers are semiconductors or insulators. Their energy gap can be above 2 eV, which is large for thermally activated conduction. Therefore, undoped conjugated polymers, such as polythiophenes and polyacetylenes, have a low electrical conductivity of around 10^{-10} to 10^{-8} S/cm. Their electrical conductivity can increase by several orders of magnitude up to values of around 0.1 S/cm, even at a very low level of doping (<1 %) [132].

Although possessing a relatively low electrical conductivity, the intrinsically low thermal conductivity of polymers, which is usually 1–3 orders of magnitude lower than for inorganics [133, 134] (usually in the range of 0.1–1 W/(m K)) makes them potential candidates for high-performance TE applications. In addition, their thermal conductivity mainly depends on their chemical compositions [135–139], thereby offering an opportunity for realizing higher *ZT* via tuning the power factor without heavily increasing thermal conductivity. It has theoretically been shown that under certain conditions, some quasi 1D organic crystal may have a *ZT* of 20 at room temperature [140]. In addition, the organic TE materials possess light weight, large surface areas, good flexibility, and can be prepared or modified in solution. Their application temperature is around room temperature. These properties agree well with the requirements of future applications that are geared toward personal and portable polymer-based flexible electronics [141–145]. Also, their well-investigated carbon or organic chemistry provides a good theoretical basis for these materials.

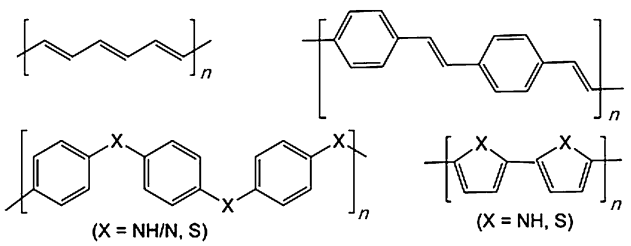

Fig. 15 Chemical structures of some conducting polymers. From top left clockwise: polyacetylene; polyphenylene vinylene; polypyrrole (X = NH) and polythiophene (X = S); and polyaniline (X = NH/N) and polyphenylene sulfide (X = S)

As described above, the weakness of organic TE materials mainly comes from their low power factor. Similar to inorganic TE materials, there exists a trade-off between their electrical conductivity and their Seebeck coefficient. For more details on the theory and mechanisms of polymer TE materials, there are already a few good reviews [146, 147], including the latest one published by He et al. [148] in 2013. Here, we briefly introduce some breakthroughs in this area. Table 1 roughly summarizes the TE performance for eight polymers up to 2010.

In 2011, Yu et al. [151] improved the TE performance of poly(3,4-ethylenedioxythiophene):poly(styrenesulfonate) (PEDOT:PSS) by addition of different concentrations of single-wall carbon nanotubes, resulting in a large TE power factor in the in-plane direction of the composites (-160 μW/(m K^2)) and high electrical conductivity (105 S/m) at room temperature. These properties make the composites very promising for various electronic applications. Although the *ZT* of their material was unavailable, their work suggested that the addition of carbon nanomaterials (graphene sheets, carbon nanotubes (CNTs), and fullerene) into organic TE materials is a good way to improve their electrical conductivity.

Chen et al. [152] investigated the electrical and thermal transport properties of a novel macro three-dimensional (3D) CNT network (as shown in Fig. 16). They found that its electrical conductivity could be adjusted through a convenient gas-fuming doping process. For example, when doped with potassium (K), the original p-type CNT network could be converted into an n-type semiconductor with a changed electrical conductivity, while iodine (I_2) doping enhanced its electrical conductivity. They used the modified CNTs to improve the TE performance of polyaniline (PANI). This work provides a good example of fabrication of low-cost polymer-based TE materials.

Another two kinds of promising organic TE materials are polyacetylene and poly(3,4-ethylenedioxythiophene).

Table 1 The electrical conductivity, Seebeck coefficient, thermal conductivity, and *ZT* of various polymers [149]

Polymer	σ (S/cm)	S (μV/K)	κ (W/(m K))	*ZT* at 300 K
Polyacetylene	4,990–11,560	11.4–28.4	0.7	0.047–0.38
Polypyrrole	100	12	0.1–0.2	0.002
Polyaniline	7,000	7	0.1–0.2	0.051
Polythiophene	100	21	0.1–0.2	0.0066
Poly(paraphenylene)	10^{-5}	12	0.1–0.2	2.1×10^{-10}
Poly(*p*-phenylenevinylene)	10^{-5}	7	0.1–0.2	7.2×10^{-11}
Poly(carbazolenevinylene)	0.005	230	0.1–0.2	8×10^{-5}
PEDOT:PSS	55	13	0.1–0.2	0.0014
PEDOT:PSS[a]	900	75	0.24	0.42

[a] Date from ref. [150]

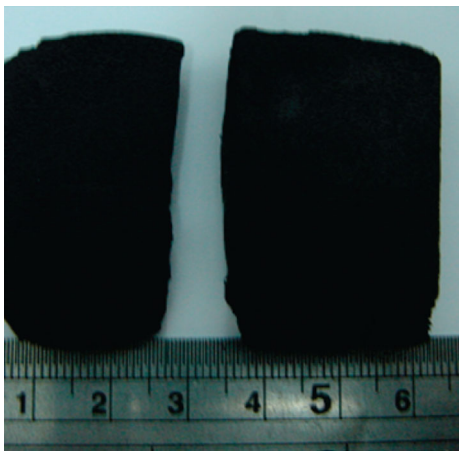

Fig. 16 (Color online) 3D CNT Network. Reprinted with permission from [152], Copyright 2012, American Chemical Society

In doped acetylene [149], a *ZT* of 0.38 has been observed at room temperature, but this material is not even stable in air. In poly(3,4-ethylenedioxythiophene), a *ZT* of 0.25 has been measured at room temperature, and this material is air stable [153].

Another possible solution to the low power factor of polymer-based TE materials is the formation of hybrids or composites by adding conductive inorganic nanomaterials. Toshima et al. [154] tried to directly mix polyaniline with pristine Au nanoparticles and improved its electrical conductivity to 350 S/cm at 50 °C while keeping a relatively high Seebeck coefficient. They also added dodecanethiol protected Au nanoparticles (NPs) to improve the electrical conductivity of poly(3,4-ethylenedioxythiophene) film to increase its *ZT* from 0.0062 to 0.0163 at 50 °C. Du et al. [155] have published a good review on inorganic–organic hybrid TE materials.

According to their calculated results, Kim et al. [150, 156] concluded that reducing the dopant concentration (represented by the product of the subunit volume ratio and the subunit concentration ratio) is as important as optimizing carrier concentration to maximize *ZT* for organic semiconductors. This is because the exponential dependence of carrier mobility on dopant volume leads to a variation in over-typical doping concentrations in organic semiconductors, which is much larger than the variation in over-typical doping concentrations in inorganic semiconductors. By employing this strategy to dope poly(styrenesulphonate) in poly(3,4-ethylenedioxythiophene), they achieved a *ZT* of 0.42 at room temperature. This is the highest *ZT* obtained among organic semiconductor-based TE materials at present.

4 Summary

We have summarized the recent advances in both inorganic and organic TE materials from experimental and theoretical perspectives. Detailed *ZT* values for these TE materials were listed in Table 2. In most cases, the enhancement of TE performance is attributed to the introduction of nanostructures into the host matrix, including nano-inclusions, nanocomposites, nanowires, nanopores, nanograins, point defects, etc. Therefore, the development of TE performance is reliant on the advances in nano-science and nanotechnology.

Nanostructures can significantly reduce thermal conductivity by enhancing the phonon scattering of materials. Unfortunately, the decrease in thermal conductivity is at the cost of carrier mobility in some cases. The deterioration in carrier mobility results from the disturbance arising from various types of phonon scattering, such as the scattering between the nanostructure and the charge carriers. In order to increase carrier mobility without raising thermal conductivity, reconstructing the electron transport channel is necessary (i.e., increasing the ratio of ordered structure). A good example of such reconstruction is modulation doping. Although the current TE nanomaterials show high performance, they face the following challenges: (1) large-scale

Table 2 Some representatives of high-performance inorganic TE materials

Type	Material	Temperature (K)	*ZT*	Reference	Mechanism
Metal chalcogenides	$PbTe(SrTe)_4Na_2$	915	2.2	[50]	Full scale phonon scattering
	Bi_2Te_3–Sb_2Te_3	300	2.4	[56]	Superlattice
Superionic conductor	p-type $Cu_{2-x}Se$	1,000	1.6	[67]	Structure, dope, phase transition
	n-type $Cu_{2-x}Se$	400	2.3	[68]	
Oxides	$SrTiO_3$	~300	2.4	[79]	Superlattice
Silicon based	Silicon	1,275	0.7	[86]	Nanowire
	SiGe	800	2	[95]	
	$Mg_2Si_{0.4}Sn_{0.6}$	800	1.1	[110]	Solid solution
PGEC	$(Sr, Ba, Yb)_{0.07}Co_4Sb_{12}$	800	1.8	[120]	Dope, nanostructure
	$Ba_8Ga_{16}Ge_{30}$	900	1.35	[122]	Extrinsic to intrinsic transition
	$Zr_{0.5}Hf_{0.5}CoSb_{0.8}Sn_{0.2}$	973	0.8	[129]	Nano inclusion

preparation of size, shape, and composition tunable nanomaterials; (2) poor stability of nanostructures, as they can be destroyed during compression into highly dense pellets at high temperature or high pressure; (3) although 1D nanowires and 2D nanosheets provide excellent samples for investigating TE properties on the individual material level, large-scale fabrication of TE devices from them without destroying the structure for practical application is a big issue; and (4) the formation of ordered nanostructures as desired.

Similar to TE nanomaterials, bulk superionic conductors can also have high *ZT* values (e.g., Cu_2Se has a *ZT* of 1.5 at 1,000 K) due to their unique PLEC properties. The PLEC is attributed to the fast movement of cations (or anions in anionic superionic conductors) and their deficiency. The introduction of nanotechnology into this field would significantly boost their TE performance and spark their practical application, as producing them in nanostructured form not only can reduce their thermal conductivity but also can promote high electrical conductivity due to higher deficiency and faster movement of cations (or anions).

It should be noted that most TE materials have issues of low *ZT*, high cost, or environmental unfriendliness. Many high *ZT* materials produced in the laboratory have no commercial potential due to the difficulties in large-scale preparation, as well as high fabrication cost and poor stability. In order to commercialize those mid-*ZT* materials with low price and high stability, more attention should be paid to the design and optimization of high-performance TE devices, while great efforts are devoted to improving their *ZT*. This is because the real conversion efficiency of TE devices is much lower than the theoretical value, even if the *ZT* of a TE material is as high as 4 [157].

In order to improve the overall energy conversion efficiency, TE devices are combined with other devices such as solar cells. Many TE materials can be also used in solar cells, such as Si and metal chalcogenides. Recently, Kraemer et al. [158] reported a flat-panel solar TE generator (STEG) with a system efficiency of 4.6 %–5.2 % generated from a temperature difference of 180 °C (T_c = 20 °C, T_h = 200 °C). This efficiency is 7–8 times higher than the best value previously reported. Wang et al. [159] developed a novel photovoltaic-TE (PV-TE) hybrid device composed of a series-connected dye-sensitized solar cell (DSSC), a solar selective absorber, and a TE generator. The overall conversion efficiency is over 13 %. This work highlights the potential of hybrid devices in conversion of abundant solar energy into electricity. The wide application of clean solar energy would significantly reduce fossil fuel consumption, our CO_2 footprint, and environmental deterioration, so the use of multiple energy conversion devices to yield maximal output would be an important direction in this area.

Acknowledgments C. Han gratefully acknowledges the Chinese Scholarship Council (CSC) for his scholarship. Z. Li acknowledges support from Australian Research Council (ARC) through the Discovery Project DP130102699. S. Dou is grateful for support from the Baosteel-Australia Research Centre (BARC) through the Project BA110011 and ARC through the Linkage Project LP120200289. The authors also thank Dr. T. Silver for polishing the manuscript.

References

1. Bell LE (2008) Cooling, heating, generating power, and recovering waste heat with thermoelectric systems. Science 321:1457–1461
2. Shakouri A, Zebarjadi M, Volz S (eds) (2009) Thermal nanosystems and nanomaterials. Springer, Heidelberg
3. Kraemer D, Poudel B, Feng HP et al (2011) High-performance flat-panel solar thermoelectric generators with high thermal concentration. Nat Mater 10:532–538
4. Loffe AF (1960) Physics of semiconductors. Academic Press, New York
5. Majumdar A (2004) Thermoelectricity in semiconductor nanostructures. Science 303:777–778
6. Pichanusakorn P, Bandaru P (2010) Nanostructured thermoelectrics. Mater Sci Eng 67:19–63

7. Shakouri A (2011) Recent developments in semiconductor thermoelectric physics and materials. Annu Rev Mater Res 41:399–431
8. Snyder GJ, Toberer ES (2008) Complex thermoelectric materials. Nat Mater 7:105–114
9. Heremans JP, Jovovic V, Toberer ES et al (2008) Enhancement of thermoelectric efficiency in PbTe by distortion of the electronic density of states. Science 321:554–557
10. Liang WJ, Hochbaum AI, Fardy M et al (2009) Field-effect modulation of Seebeck coefficient in single PbSe nanowires. Nano Lett 9:1689–1693
11. Kittel C (2005) Introduction to solid state physics. Chemical Industry Press, Beijing
12. Slack GA, Rowe DM, Boca R (eds) (1995) Handbook of thermoelectrics. CRC Press, Boca Raton
13. Hicks LD, Dresselhaus M (1993) Figure of merit of a one-dimensional conductor. Phys Rev B 47:16631–16634
14. Hicks LD, Dresselhaus M (1993) Effect of quantum well structures on the thermoelectric figure of merit. Phys Rev B 47:12727–12731
15. Harman TC, Walsh MP, LaForge BE et al (2005) Nanostructured thermoelectric materials. J Electron Mater 34:L19–L22
16. He J, Liu YF (2011) Oxide thermoelectrics: the challenges, progress, and outlook. J Mater Res 26:1762–1772
17. Bubnova O, Crispin X (2012) Towards polymer-based organic thermoelectric generators. Energy Environ Sci 5:9345–9362
18. Rowe DM (1986) Recent developments in thermoelectric materials. Appl Energy 24:139–162
19. Sootsman JR, Chung DY, Kanatzidis MG (2009) New and old concepts in thermoelectric materials. Angew Chem Int Ed 48:8616–8639
20. Liu WS, Yan X, Chen G et al (2012) Recent advances in thermoelectric nanocomposites. Nano Energy 1:42–56
21. Li Z, Sun Q, Yao XD et al (2012) Semiconductor nanowires for thermoelectrics. J Mater Chem 22:22821–22831
22. Li Z, Kornowski A, Myalitsin A et al (2008) Formation and function of bismuth nanocatalysts for the solution–liquid–solid synthesis of CdSe nanowires. Small 4:1698–1702
23. Li Z, Kurtulus Ö, Nan F et al (2009) Controlled synthesis of CdSe nanowires by solution–liquid–solid method. Adv Funct Mater 19:3650–3661
24. Li Z, Cheng LN, Sun Q et al (2010) Diluted magnetic semiconductor nanowires prepared by the solution–liquid–solid method. Angew Chem Int Ed 49:2777–2781
25. Li Z, Ma X, Sun Q et al (2010) Synthesis and characterization of colloidal core–shell semiconductor nanowires. Eur J Inorg Chem 27:4325–4331
26. Li Z, Du AJ, Sun Q et al (2011) Cobalt-doped cadmium selenide colloidal nanowires. Chem Commun 47:11894–11896
27. Li Z, Du AJ, Sun Q et al (2012) Field-effect transistors fabricated from diluted magnetic semiconductor colloidal nanowires. Nanoscale 4:1263–1266
28. Wang YJ, Wilkinson DP, Zhang J (2011) Noncarbon support materials for polymer electrolyte membrane fuel cell electrocatalysts. Chem Rev 111:7625–7651
29. Gewirth AA, Thorum MS (2010) Electroreduction of dioxygen for fuel-cell applications: materials and challenges. Inorg Chem 49:3557–3566
30. Zhang GQ, Finefrock S, Liang DX et al (2011) Semiconductor nanostructure-based photovoltaic solar cells. Nanoscale 3: 2430–2443
31. Gratzel M (2001) Photoelectrochemical cells. Nature 414:338–344
32. Tarascon JM, Armand M (2001) Issues and challenges facing rechargeable lithium batteries. Nature 414:359–367
33. Li H, Wang ZX, Chen LQ et al (2009) Research on advanced materials for Li-ion batteries. Adv Mater 21:4593–4607
34. Ikoma K, Munekiyo M, Furuya K et al (1999) Thermoelectric generator for gasoline engine vehicles using Bi_2Te_3 modules. J Jpn Inst Met 63:1475–1478
35. Lv HY, Liu HJ, Shi J et al (2013) Optimized thermoelectric performance of Bi_2Te_3 nanowires. J Mater Chem A 1: 6831–6838
36. Tang XF, Xie WJ, Li H et al (2007) Preparation and thermoelectric transport properties of high-performance p-type Bi_2Te_3 with layered nanostructure. Appl Phys Lett 90:012102
37. Venkatasubramanian R, Siivola E, Colpitts T et al (2001) Thin-film thermoelectric devices with high room-temperature figures of merit. Nature 413:597–602
38. Harman TC, Taylor PJ, Walsh MP et al (2002) Quantum dot superlattice thermoelectric materials and devices. Science 297:2229–2232
39. Lalonde A, Pei YZ, Snyder GJ (2011) Reevaluation of $PbTe_{1-x}I_x$ as high performance n-type thermoelectric material. Energy Environ Sci 4:2090–2096
40. Pei YZ, Lalonde A, Iwanaga S et al (2011) High thermoelectric figure of merit in heavy hole dominated PbTe. Energy Environ Sci 4:2085–2089
41. Pei YZ, Shi XY, Lalonde A et al (2011) Convergence of electronic bands for high performance bulk thermoelectrics. Nature 473:66–69
42. He JQ, Sootsman JR, Girard SN et al (2010) On the origin of increased phonon scattering in nanostructured PbTe based thermoelectric materials. J Am Chem Soc 132:8669–8675
43. Hsu KF, Loo S, Guo F et al (2004) Cubic $AgPb_mSbTe_{2+m}$: bulk thermoelectric materials with high figure of merit. Science 303:818–821
44. Poudeu PFP, D'Angel JJ, Downey AD et al (2006) High thermoelectric figure of merit and nanostructuring in bulk p-type $Na_{1-x}Pbm SbyTe_{m+2}$. Angew Chem Int Ed 45:3835–3839
45. Biswas K, He JQ, Zhang QC et al (2011) Strained endotaxial nanostructures with high thermoelectric figure of merit. Nat Chem 3:160–166
46. Sootsman JR, Kong HJ, Uher C et al (2008) Large enhancements in the thermoelectric power factor of bulk PbTe at high temperature by synergistic nanostructuring. Angew Chem Int Ed 47:8618–8622
47. Pei YZ, Lensch-Falk J, Tobber ES et al (2011) High thermoelectric performance in PbTe due to large nanoscale Ag_2Te precipitates and La doping. Adv Funct Mater 21:241–249
48. Ahn K, Han MK, He JQ et al (2010) Exploring resonance levels and nanostructuring in the PbTe–CdTe system and enhancement of the thermoelectric figure of merit. J Am Chem Soc 132:5227–5235
49. Androulakis J, Lin CH, Kong HJ et al (2007) Spinodal decomposition and nucleation and growth as a means to bulk nanostructured thermoelectrics: enhanced performance in $Pb_{1-x}Sn_xTe$–PbS. J Am Chem Soc 129:9780–9788
50. Kanishka B, He JQ, Ivan DB (2012) High-performance bulk thermoelectrics with all-scale hierarchical architectures. Nature 489:414–418
51. Ibanez M, Zamani R, Gorsse S et al (2013) Core-shell nanoparticles as building blocks for the bottom-up production of functional nanocomposites: pbTe–PbS thermoelectric properties. ACS Nano 7:2573–2586
52. Rogacheva EI, Tavrina TV, Nashchekina ON et al (2002) Quantum size effects in PbSe quantum wells. Appl Phys Lett 80:2690–2692
53. Wang H, Pei YZ, Lalonde AD et al (2011) Heavily doped p-type PbSe with high thermoelectric performance: an alternative for PbTe. Adv Mater 23:1366–1370
54. Zhang QY, Wang H, Liu WS et al (2012) Enhancement of thermoelectric figure-of-merit by resonant states of aluminium doping in lead selenide. Energy Environ Sci 5:5246–5251

55. Johnsen S, He JQ, Androulakis J et al (2011) Nanostructures boost the thermoelectric performance of PbS. J Am Chem Soc 133:3460–3470
56. Venkatasubramanian R, Siivola E, Colpitts T et al (2001) Thin-film thermoelectric devices with high room-temperature figures of merit. Nature 413:597–602
57. Poudel B, Hao Q, Ma Y et al (2008) High-thermoelectric performance of nanostructured bismuth antimony telluride bulk alloys. Science 320:634–638
58. Xie WJ, He J, Kang HJ et al (2010) Identifying the specific nanostructures responsible for the high thermoelectric performance of $(Bi, Sb)_2Te_3$ nanocomposites. Nano Lett 10:3283–3289
59. Liu WS, Zhang QY, Lan YC et al (2011) Thermoelectric property studies on Cu-doped n-type $Cu_xBi_2Te_{2.7}Se_{0.3}$ nanocomposites. Adv Energy Mater 1:577–587
60. Ko DK, Kang YJ, Murray CB (2011) Enhanced thermopower via carrier energy filtering in solution-processable Pt–Sb_2Te_3 nanocomposites. Nano Lett 11:2841–2844
61. Liu DW, Li JF, Chen G et al (2011) Effects of SiC nanodispersion on the thermoelectric properties of p-type and n-type Bi_2Te_3-based alloys. J Electron Mater 40:992–998
62. Yan X, Poudel B, Ma Y et al (2010) Experimental studies on anisotropic thermoelectric properties and structures of n-type Bi_2Te_2·7Se0.3. Nano Lett 10:3373–3378
63. Ferdows A, Roger L (2010) Thermoelectric properties of Bi_2Te_3 atomic quintuple thin films. Appl Phys Lett 97:18078
64. Zhang GQ, Kirk B, Jauregui LA et al (2012) Rational synthesis of ultrathin n-type Bi_2Te_3 nanowires with enhanced thermoelectric properties. Nano Lett 12:56–60
65. Zhang GQ, Fang HY, Yang HR et al (2012) Design principle of telluride-based nanowire heterostructures for potential thermoelectric applications. Nano Lett 12:3627–3633
66. Li AH, Shahbazi M, Zhou SH et al (2010) Electronic structure and thermoelectric properties of Bi_2Te_3 crystals and graphene-doped Bi_2Te_3. Thin Solid Films 518:e57–e60
67. Liu HL, Shi X, Xu FF et al (2012) Copper ion liquid-like thermoelectrics. Nat Mater 11:422–425
68. Liu HL, Yuan X, Lu P et al (2013) Ultrahigh thermoelectric performance by electron and phonon critical scattering in $Cu_2Se_{1-x}I_x$. Adv Mater 25:6607–6612
69. Zhu JJ, Palchik O, Chen SG et al (2000) Microwave assisted preparation of CdSe, PbSe, and $Cu_{2-x}Se$ nanoparticles. J Phys Chem B 104:7344–7347
70. Filippo E, Manno D, Serra A (2012) Synthesis and growth mechanism of dendritic $Cu_{2-x}Se$ microstructures. J Alloys Compd 538:8–10
71. Shen HB, Wang HZ, Yuan H et al (2012) Size-, shape-, and assembly-controlled synthesis of $Cu_{2-x}Se$ nanocrystals via a non-injection phosphine-free colloidal method. Cryst Eng Commun 14:555–560
72. Chen HH, Zou RJ, Wang N et al (2011) Lightly doped single crystalline porous Si nanowires with improved optical and electrical properties. J Mater Chem 21:3053–3059
73. Xiao C, Xu J, Li K et al (2012) Superionic phase transition in silver chalcogenide nanocrystals realizing optimized thermoelectric performance. J Am Chem Soc 134:4287–4293
74. Xiao C, Qin XM, Zhang J et al (2012) High thermoelectric and reversible p-n-p conduction type switching integrated in dimetal chalcogenide. J Am Chem Soc 134:18460–18466
75. Zhang Y, Hu CG, Zheng CH et al (2010) Synthesis and thermoelectric property of $Cu_{2-x}Se$ nanowires. J Phys Chem C 114:14849–14853
76. Terasaki I (2011) High-temperature oxide thermoelectrics. J Appl Phys 110:053705
77. Misture S, Edwards D (2012) High-temperature oxide thermoelectrics. Am Ceram Soc Bull 91:24–27
78. Noudem JG, Kenfaui D, Chateigner D et al (2011) Granular and lamellar thermoelectric oxides consolidated by spark plasma sintering. J Electron Mater 40:1100–1106
79. Ohta H, Kim SW, Mune Y et al (2007) Giant thermoelectric seebeck coefficient of a two-dimensional electron gas in $SrTiO_3$. Nat Mater 6:129–134
80. Jood P, Mehta RJ, Zhan YL et al (2011) Al-doped zinc oxide nanocomposites with enhanced thermoelectric properties. Nano Lett 11:4337–4342
81. Li F, Li JF, Zhao LD et al (2012) Polycrystalline BiCuSeO oxide as a potential thermoelectric material. Energy Environ Sci 5:7188–7195
82. Li JF, Sui JH, Pei YL et al (2012) A high thermoelectric figure of merit $ZT > 1$ in Ba heavily doped BiCuSeO oxyselenides. Energy Environ Sci 5:8543–8547
83. Constantinescu G, Diez JC, Rasekh S et al (2013) New promising Co-free thermoelectric ceramic based on Ba–Fe-oxide. J Mater Sci 24:1832–1836
84. Hochbaum AI, Chen R, Delgado RD (2008) Enhanced thermoelectric performance of rough silicon nanowires. Nature 451:163–168
85. Akram IB, Yuri B, Jamil TK (2008) Silicon nanowires as efficient thermoelectric materials. Nature 451:168–171
86. Sabah KB, Richard GB, Pawan KG (2009) Nanostructured bulk silicon as an effective thermoelectric material. Adv Funct Mater 19:2445–2452
87. Lee JH, Galli GA, Grossman JC (2008) Nanoporous Si as an efficient thermoelectric material. Nano Lett 8:3750–3754
88. Yang CC, Li S (2011) Basic principles for rational design of high-performance nanostructured silicon-based thermoelectric materials. ChemPhysChem 12:3614–3618
89. Joshi G, Lee H, Lan YC et al (2008) Enhanced thermoelectric figure-of-merit in nanostructured p-type silicon germanium bulk alloys. Nano Lett 8:4670–4674
90. Wang XW, Lee H, Lan YC et al (2008) Enhanced thermoelectric figure of merit in nanostructured n-type silicon germanium bulk alloy. Appl Phys Lett 93:193121(1–4)
91. Lan YC, Minnich AJ, Chen G et al (2010) Enhancement of thermoelectric figure-of-merit by a bulk nanostructuring approach. Adv Funct Mater 20:357–376
92. Zhu GH, Pillitteri A, Dresselhaus MS et al (2009) Increased phonon scattering by nanograins and point defects in nanostructured silicon with a low concentration of germanium. Phys Rev Lett 102:196803
93. Yu B, Zebarjadi M, Wang H et al (2012) Enhancement of thermoelectric properties by modulation-doping in silicon germanium alloy nanocomposites. Nano Lett 12:2077–2082
94. Mingo N, Hauser D, Kobayashi NP et al (2009) "Nanoparticle-in-alloy" approach to efficient thermoelectrics: silicides in SiGe. Nano Lett 9:711–715
95. Lee EK, Hippalgaonkar K, Majumdar A et al (2012) Large thermoelectric figure-of-merits from SiGe nanowires by simultaneously measuring electrical and thermal transport properties. Nano Lett 12:2918–2923
96. Tritt TM (1996) Thermoelectrics run hot and cold. Science 272:1276–1277
97. Lee HJ, Cho YR, Kim IH (2011) Synthesis of thermoelectric Mg_2Si by a solid state reaction. J Ceram Process Res 12:16–20
98. Nolas GS, Sharp J, Goldsmid HJ (2000) Thermoelectrics. Springer, Berlin
99. Ikeda T, Haviez L, Li YL et al (2012) Nanostructureing of thermoelectric Mg_2Si via a nonequilibrium intermediate state. Small 8:2350–2355
100. Saravanan R, Charles RM (2009) Local structure of the thermoelectric material Mg_2Si using XRD. J Alloys Compd 479: 26–31

101. Vining CB, Rowe DM (eds) (1995) Handbook of thermoelectrics. CRC Press, New York
102. Massayasu A, Tsutomu I, Takashi N (2007) Non-wetting crystal growth of Mg_2Si by vertical Bridgman method and thermoelectric characteristics. J Cryst Growth 304:196–201
103. Jiang HY, Long HS, Zhang LM (2004) Effects of solid-state reaction synthesis processing parameters on thermoelectric properties of Mg_2Si. J Wuhan Univ Tech-Mater Sci Ed 19:55–56
104. Zhou SC, Bai CG (2011) Microwave direct synthesis and thermoelectric properties of Mg_2Si by solid-state reaction. Trans Nonferr Met Soc China 21:1785–1789
105. You SW, Kim IH (2011) Solid-state synthesis and thermoelectric properties of Bi-doped Mg_2Si compounds. Curr Appl Phys 11:S392–S395
106. Yang MJ, Zhang LM, Shen Q (2009) Nanostructuring and thermoelectric properties of bulk n-type Mg_2Si. J Wuhan Univ Tech-Mater Sci Ed 24:912–916
107. Nikhil S, Daryoosh VT (2012) The effect of crystallite size on thermoelectric properties of bulk nanostructured magnesium silicide (Mg_2Si) compounds. Appl Phys Lett 100:073107
108. Yang MJ, Shen Q, Zhang LM (2011) Effect of nanocomposite structure on the thermoelectric properties of 0.7-at% Bi-doped Mg_2Si nanocomposite. China Phys B 20:106202
109. Yang MJ, Luo WJ, Shen Q et al (2009) Synthesis of Mg_2Si nano composite and its thermoelectric properties. Rare Met Mater Eng S2:1055–1059
110. Zaitsev VK, Fedorov MI, Gurieva EA (2006) Highly effective Mg_2Si_1–xSn_x thermoelectrics. Phys Rev B 74:045207
111. Noda Y, Kon H, Furukawa Y (1992) Preparation and thermoelectric properties of $Mg_2Si_{1-x}Ge_x$ ($x = 0.0$–0.4) solid solution semiconductors. Mater Trans 33:845–850
112. Zhao D, Tian C, Tang S et al (2010) High temperature oxidation behavior of cobalt triantimonide thermoelectric material. J Alloys Compd 504:552–558
113. Zhao D, Tian C, Tang S et al (2011) High temperature sublimation behavior of antimony in $CoSb_3$ thermoelectric material during thermal duration test. J Alloys Compd 509:3166–3171
114. Hara R, Inoue S, Kaibe HT et al (2003) Aging effects of large-size n-type $CoSb_3$ prepared by spark plasma sintering. J Alloys Compd 349:297–301
115. Donald IW (1993) Preparation, properties and chemistry of glass- and glass-ceramic-to-metal seals and coatings. J Mater Sci 28:2841–2886
116. Leszczynski J, Wojciechowski TK, Malecki AL (2011) Studies on thermal decomposition and oxidation of $CoSb_3$. J Therm Anal Calorim 105:211–222
117. Sklad AC, Gaultois MW, Grosvenor AP (2010) Examination of $CeFe_4Sb_{12}$ upon exposure to air: is this material appropriate for use in terrestrial, high-temperature thermoelectric devices? J Alloys Compd 505:L6–L9
118. Mehrer H, Imre AW (2008) Diffusion and ionic conduction in oxide glasses. J Phys 106:012001
119. Shi X, Yang J, Salvador JR (2011) Multiple-filled skutterudites: high thermoelectric figure of merit through separately optimizing electrical and thermal transports. J Am Chem Soc 133:7837–7846
120. Rogl G, Aabdin Z, Schafler E et al (2012) Effect of HPT processing on the structure, thermoelectric and mechanical properties of $Sr_{0.07}Ba_{0.07}Yb_{0.07}Co_4Sb_{12}$. J Alloys Compd 537:183–189
121. Christensen M, Johnsen S, Iversen BB (2010) Thermoelectric clathrates of type I. Dalton Trans 39:978–992
122. Saramat A, Svensson G, Palmqvist AE et al (2006) Large thermoelectric figure of merit at high temperature in Czochralski-grown clathrate $Ba_8Ga_{16}Ge_{30}$. J Appl Phys 99:023708
123. Zintl E (1939) Intermetallische verbindungen. Angew Chem 52:1–6
124. Kauzlarich SM, Brown SR, Snyder GJ (2007) Zintl phases for thermoelectric devices. Dalton Trans 21:2099–2107
125. Paschen S, Pacheco V, Bentien A et al (2003) Are type-I clathrates Zintl phases and "phonon glasses and electron single crystals"? Phys B 328:39–43
126. Prokofiev A, Ikeda M, Makalkina E et al (2013) Melt spinning of clathrates: electron microscopy study and effect of composition on grain size. J Electron Mater 42:1628–1633
127. Yan X, Falmbigl M, Rogl G et al (2013) High-pressure torsion to improve thermoelectric efficiency of clathrates? J Electron Mater 42:1330–1334
128. Yang J, Li HM, Wu T et al (2008) Evaluation of half-Heusler compounds as thermoelectric materials based on the calculated electrical transport properties. Adv Funct Mater 18:2880–2888
129. Yan X, Joshi G, Liu WS et al (2011) Enhanced thermoelectric figure of merit of p-type half-Heuslers. Nano Lett 11:556–560
130. Benjamin B, Joachim B, Micheal S et al (2011) An alternative approach to improve the thermoelectric properties of half-Heusler compounds. J Electron Mater 40:702–706
131. Xie WJ, Weidenkaff A, Tang XF (2012) Recent advances in nanostructured thermoelectric half-Heusler compounds. Nanomaterials 2:379–412
132. Budnova O, Crispin X (2012) Towards polymer-based organic thermoelectric generators. Energy Environ Sci 5:9345–9362
133. Zhou YC, Wang L, Zhang H et al (2012) Enhanced high thermal conductivity and low permittivity of polyimide based composites by core-shell $Ag@SiO_2$ nanoparticle fillers. Appl Phys Lett 101:012903
134. Han ZD, Fina A (2011) Thermal conductivity of carbon nanotubes and their polymer nanocomposites: a review. Prog Polym Sci 36:914–944
135. Alaghemandi M, Gharib-Zahedi MR, Spohr E et al (2012) Thermal conductivity of polyamide-6,6 in the vicinity of charged and uncharged graphene layers: a molecular dynamics analysis. J Phys Chem C 116:14115–14122
136. Kamseu E, Nait-Ali B, Bignozzi MC et al (2012) Bulk composition and microstructure dependence of effective thermal conductivity of porous inorganic polymer cements. J Eur Ceram Soc 32:1593–1603
137. Huang XY, Iizuka T, Jiang PK et al (2012) Role of interface on the thermal conductivity of highly filled dielectric epoxy/AlN composites. J Phys Chem C 116:13629–13639
138. Yan H, Sada N, Toshima N (2002) Thermal transporting properties of electrically conductive polyaniline films as organic thermoelectric materials. J Therm Anal Calorim 69:881–887
139. He M, Ge J, Fang M et al (2010) Fabricating polythiophene into highly aligned microwire film by fast evaporation of its whisker solution. Polymer 51:2236–2243
140. Casian A, Balandin AA, Dusciac V et al (2002) Promising low-dimensional organic material for IR detectors. In: Proceedings of the 21st international conference on thermoelectrics, IEEE, Long Beach, 25–29 August, 2002
141. He M, Han W, Ge J et al (2011) All-conjugated poly(3-alkylthiophene) diblock copolymer-based bulk heterojunction solar cells with controlled molecular organization and nanoscale morphology. Energy Environ Sci 4:2894–2902
142. He M, Han W, Ge J et al (2011) Annealing effects on the photovoltaic performance of all-conjugated poly(3-alkylthiophene) diblock copolymer-based bulk heterojunction solar cells. Nanoscale 3:3159–3163
143. He M, Qiu F, Lin Z (2011) Conjugated rod-coil and rod–rod block copolymers for photovoltaic applications. J Mater Chem 21:17039–17048
144. Ge J, He M, Yang XB et al (2012) The first homochiral coordination polymer with temperature-independent piezoelectric and dielectric properties. J Mater Chem 22:19213–19216

145. Wang ZL (2012) Self-powered nanosensors and nanosystems. Adv Mater 24:280–285
146. Dubey N, Leclerc M (2011) Conducting polymers: efficient thermoelectric materials. J Polym Sci B: Polym Phys 49:467–475
147. Njoroge JL (2010) High thermoelectric efficiency achieved in polymer-nanocomposites. Mater Res Bull 35:909–910
148. He M, Qiu F, Lin ZQ (2013) Towards high-performance polymer-based thermoelectric materials. Energy Environ Sci 6:1352–1361
149. Xuan Y, Liu X, Desbief S et al (2010) Thermoelectric properties of conducting polymers: the case of poly(3-hexylthiophene). Phys Rev B 82:15454–15457
150. Kim GH, Shao L, Zhang K et al (2013) Engineered doping of organic semiconductors for enhanced thermoelectric efficiency. Nat Mater 12:719–723
151. Yu CH, Choi KW, Yin L et al (2011) Light-weight flexible carbon nanotube based organic composites with large thermoelectric power factors. ACS Nano 5:7885–7892
152. Chen JK, Gui XC, Wang ZW (2012) Superlow thermal conductivity 3D carbon nanotube network for thermoelectric applications. Appl Mater Interface 4:81–86
153. Wang YY, Cai KF, Yin JL et al (2011) In situ fabrication and thermoelectric properties of PbTe–polyaniline composite nanostructures. J Nanopart Res 13:533–536
154. Toshima N, Jiravanichanun N, Marutani H (2012) Organic thermoelectric materials composed of conducting polymers and metal nanoparticles. J Electron Mater 41:1735–1742
155. Du Y, Shen SZ, Cai KF et al (2013) Research progress on polymer–inorganic thermoelectric nanocomposite materials. Prog Polym Sci 42:1882–1887
156. Kim GH, Pipe KP (2012) Thermoelectric model to characterize carrier transport in organic semiconductors. Phys Rev B 86:085208
157. Cronin BV (2009) An inconvenient truth about thermoelectrics. Nat Mater 8:84–85
158. Kraemer D, Poudel B, Feng HP et al (2011) High-performance flat-panel solar thermoelectric generators with high thermal concentration. Nat Mater 10:532–538
159. Wang XW, Lee H, Lan YC et al (2008) Enhanced thermoelectric figure of merit in nanostructured n-type silicon germanium bulk alloy. Appl Phys Lett 93:193121